Journal of Fluids and Structures (1998) **12,** 591–613
Article No. fl980156

HELICAL WAVE OSCILLATIONS IN A ROW OF CYLINDERS IN A CROSS-FLOW†

M. Thothadri‡ and F. C. Moon

School of Mechanical and Aerospace Engineering, Cornell University
Ithaca, NY 14853, U.S.A.

(Received 3 February 1997 and in revised form 12 January 1998)

The dynamics of a row of cylinders oscillating in a cross-flow is investigated using experiments and analysis. Through experiments, a bifurcation diagram that classifies the nonlinear behavior of the cylinder row is obtained. The experiments show that the stability of the cylinder row is lost through a sub-critical Hopf bifurcation. As the number of oscillating cylinders is increased, the experiments show that the critical flow velocity decreases. To analyze the motions of the cylinder system, a linear model is studied using wave propagation theory. The motion-dependent fluid forces acting on the cylinders are assumed to be linear functions of the relative motion between adjacent cylinders only. A system identification technique is used to measure some of the fluid force coefficients. The analysis of the model shows the presence of modal patterns for the cylinder row that are analogous to standing helical waves in a string. The modes predicted by the linear model are similar to the experimentally observed nonlinear modes. The co-existence of more than one stable mode (limit cycle) for a range of flow velocities, not predictable by the linear model, is a noteworthy nonlinear phenomenon observed in the experiments of this study.

1. INTRODUCTION

It is well known that an array of cylinders placed in a uniform cross-flow undergoes oscillations beyond a certain threshold flow velocity. In various engineering systems, such oscillations can lead to structural damage. For example, flow-excited oscillations can cause damaging impacts and fatigue failure in heat exchanger systems. Thus, it is important to be able to characterize the dynamics of such systems and predict the onset of potentially destructive oscillatory behavior.

A number of experimental and analytical studies have been carried out to understand the dynamics of cylinders in a uniform cross-flow (Roberts 1966; Connors 1970; Blevins 1977; Chen 1978, 1983, 1987; Tanaka & Takahara 1980; Lever & Weaver 1982; Païdoussis *et al.* 1985; Païdoussis & Price 1988; Chen *et al.* 1993). Price (1995) provides an extensive review of all the models of fluidelastic instability for cylinder arrays in cross-flow. This review compares various models and experimental data while laying emphasis on the physics of the different instability mechanisms. Païdoussis (1987) provides a review of the work in fluidelastic instabilities due to internal flow, external axial flow, annular flow and

†Supported in part by a grant from Department of Energy, Division of Basic Engineering Sciences
‡Graduate Research Assistant, Department of Theoretical and Applied Mechanics

0889-9746/98/050591 + 23 $30.00

cross-flow. A similar review on fluid-elastic instabilities due to cross-flow is provided by Weaver & Fitzpatrick (1987). Chen (1989) gives an overview to resolve some of the confusion and misunderstandings regarding the determination of critical flow velocity and the effect of various parameters.

In many nonlinear system [e.g. Moon & Holmes (1979)], the spatial modes are close to the linear modes even when the temporal behavior is far from linear. To explore this issue of spatial modes was one of the goals of this study. Most of the work in this field to date has focussed on identifying the instability mechanisms and determining the critical flow velocity with less emphasis on fully understanding the modal patterns of the cylinder oscillations. The specific aims of this study have been to use experiments to (i) characterize the global dynamics of the cylinders in the cross-flow and (ii) develop a mechanical model to capture the essential modal behavior of the cylinders. To describe the global behavior, we obtain (a) a bifurcation diagram (cylinder oscillation amplitude versus flow velocity); (b) the critical flow velocity; (c) the effect of the number of cylinders on critical flow velocity; and (d) the modal patterns of the cylinder row in limit-cycle oscillations, for different flow regimes (interval of flow velocities). We find that the stability of the cylinder row is lost through a sub-critical Hopf bifurcation. These sub-critical Hopf bifurcations are dangerous in practice because damaging large amplitude oscillations may be induced at much lower flow velocities than those predicted by linear models.

To describe the modal patterns of the coupled n-cylinder periodic structure, we have developed a linear wave propagation model. In addition, we have devised a novel technique for measuring the fluid forces required by the model using system identification theory. This model shows that the modal pattern of the coupled system of cylinders is analogous to the propagation of helical waves along a string; such waves also arise in electro-mechanical dynamics (Woodson & Melcher 1968). Moreover, the model predicts that for this system where the instability is governed by fluid-stiffness forces, helical wave behavior is the only possible modal pattern.

2. EXPERIMENTAL SET-UP

The wind tunnel in this study is a standard blower type, low turbulence air tunnel powered by an AC motor. The air velocity in the test-section is controlled by adjusting the drive motor speed by a variable frequency controller. The maximum turbulence level of the wind tunnel is 0·23% and the boundary layer thickness is less than 5% of the width of the test-section for the range of the flow velocities used in this study. The maximum air speed of the wind tunnel is 14 m/s (without the cylinders) but for the experiments conducted in this study with the cylinder row, the upstream flow velocity was kept below 8·5 m/s. Muntean (1995) provides more details on the wind-tunnel characteristics and performance tests.

The test-section is 915 mm long and is made of Plexiglass. Figure 1 shows two views of the test-section and the row of cylinders. The pitch to diameter ratio (P/D) is 1·35. For tube arrays with P/D greater than 1·5, it is known that vortex shedding plays a significant role (Blevins 1977). In this study, the P/D ratio has been chosen so that vortex-induced vibrations can be avoided. The flow profile upstream of the cylinder row, measured using a pitot-static tube and a pressure transducer, was found to be uniform across the cylinder row for various speeds of the drive motor (Thothadri 1996). The setup has reflection symmetry about the y–z plane of the central cylinder under no-flow conditions.

Fixed cylinders at the ends of the cylinder row are solid 19 mm O.D. (outer diameter) aluminum rods and are bolted, top and bottom, to the structure containing the cylinders,

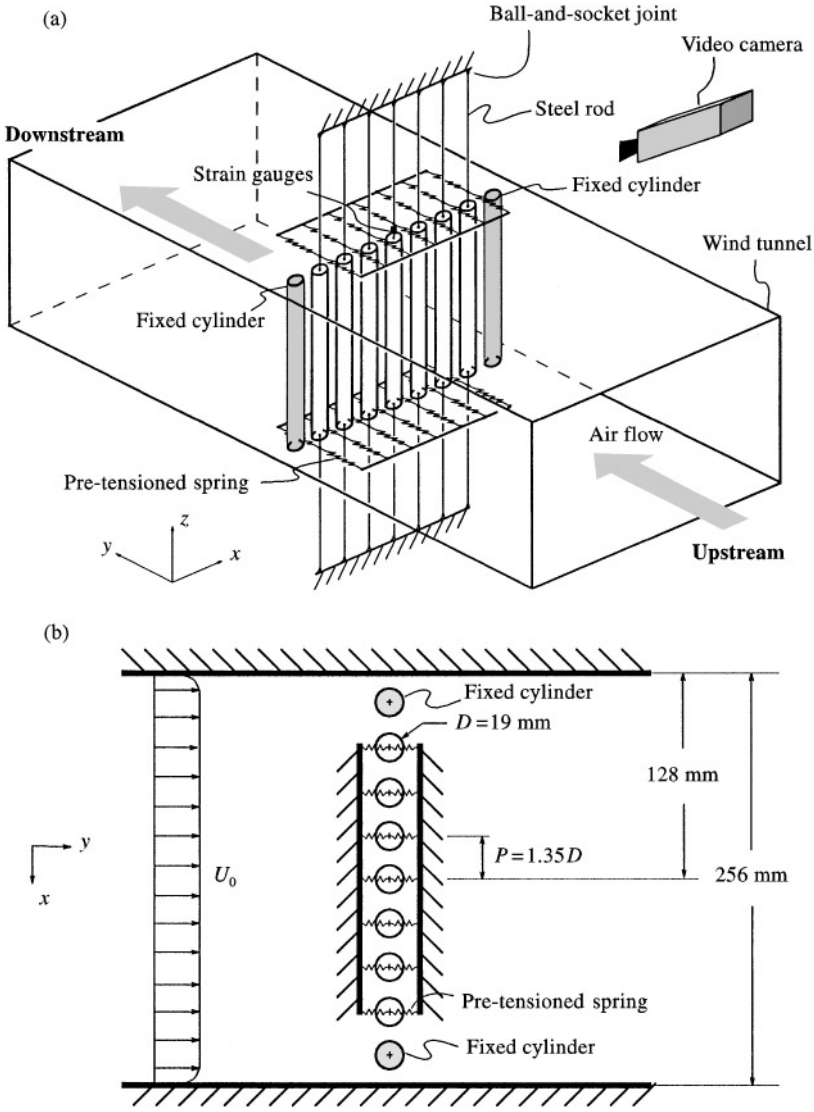

Figure 1. (a) Sketch of the test-section. (b) Top view of the cylinder row in the test-section. The air-flow between the cylinders contributes to the coupling between them; no structural coupling exists. Only the central cylinder is instrumented.

holding the entire structure in place. Each of the oscillating cylinders is made of a hollow Plexiglass tube 256 mm long with 19 mm O.D. and 16 mm I.D. Each tube has mass per unit length of 0·23 kg/m. The ends of each oscillating cylinder are sealed with caps. A 915 mm long, 1·6 mm diameter steel rod passes through these caps and supports the tube. The top end of this rod is connected to a ball-and-socket joint and the bottom end is connected to a ball-and-socket roller joint that allows vertical motion of the lower end of the rod. Each oscillating cylinder has two degrees of freedom, in-line and transverse to the flow. The restoring forces for motions in the in-line and transverse directions are provided by the extensions of the pre-tensioned springs. The contribution of the steel rod supporting the

tube to the restoring force is small. The extension of the springs attached to the cylinders can be increased or decreased to adjust the equilibrium position of the cylinders in the in-line direction. This flexibility, in addition to permitting maintenance of cylinder alignment, provides a way to compensate for the constant drag forces which are ignored in the model.

The natural frequency of the cylinders in the in-line direction (f_y) is 7·4 Hz (relative error is 2%) and 6·8 Hz (relative error is 3%) in the transverse direction (f_x). The transverse natural frequency differs† from the in-line natural frequency by about 9% and this difference prevents resonant coupling between them. The damping ratio in still air was found to be close to $\delta = 0{\cdot}013$ in both directions (relative error is 7·5%).

We obtained the response of the central cylinder by mounting two pairs of strain gauges on the steel rod supporting the cylinder. The remaining cylinders were not instrumented. The gauges were used in conjunction with Wheatstone-bridge circuits to obtain the bending strains in the rod. The cylinder displacements were obtained by calibrating these bending strains. Analog filtering of the signal was done using a 25 Hz low-pass Bessel filter. The output was recorded and analyzed with a Nicolet Model 4094C and an HP 3562A Dynamic Signal Analyzer. The recorded output was down-loaded into Sun Workstations, where all the analysis was carried out using MATLAB. For system Identification, the displacement signals were further filtered within MATLAB's Signal Processing Toolbox. We obtained the modal patterns of the cylinder row using a video camera.

3. EXPERIMENTAL RESULTS

We present the principal experimental results in this section. Note that we use a nondimensional form of the flow velocity called the reduced flow velocity, $U_r (= U/f_y D)$, where U is the mean gap flow velocity, f_y is the natural frequency of the cylinder in the in-line (y) direction and D is the diameter of the cylinder.

3.1. Global Characterization

The response of each cylinder is induced by the cross-flow and influenced by its interactions with the other cylinders. In our experiments, we quantify only the response of the central cylinder. We define *amplitude* as the maximum radial displacement of the central cylinder from its equilibrium position. (Note that all of the seven cylinders can oscillate in any direction in the x–y plane.)

The bifurcation diagram of Figure 2(a), shows the amplitude of central cylinder oscillations as a function of flow velocity. We found that the stability of the cylinder row is lost through a sub-critical Hopf bifurcation. We define the critical flow velocity U_{cr} as the lowest flow velocity for which the small-amplitude turbulent buffeting of the cylinder row grows, after sufficient time, into large-amplitude limit-cycle oscillations. Previously, Païdoussis *et al.* (1993) reported that a rotated array in a cross-flow loses stability through a supercritical Hopf bifurcation, and Muntean (1995) showed that a single cylinder in a row of rigid

†As the natural extension of the springs is in the in-line direction, the difference in the two natural frequencies results from the nonlinear restoring force for motions in the transverse direction. An approximate analytical estimate gives $f_y \approx 7{\cdot}3$ Hz and $f_x \approx 0{\cdot}85 f_y$ for transverse motions of the order of 25% of the equilibrium extension of the spring.

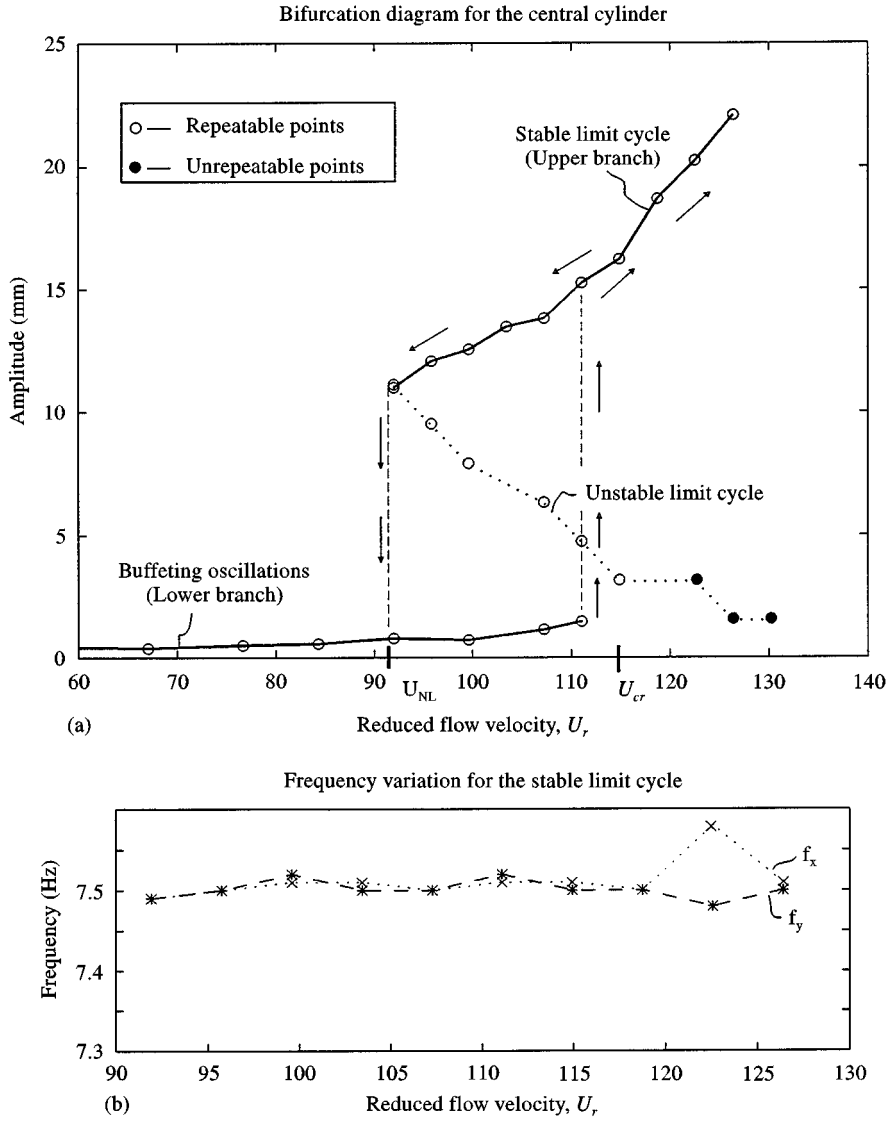

Figure 2. (a) Bifurcation diagram. The amplitude of the oscillations of the *central* cylinder in a row of seven vibrating tubes is shown versus the reduced flow velocity, U_r. A sub-critical Hopf bifurcation occurs as the reduced flow velocity is increased past the critical value of approximately 115. This bifurcation diagram was obtained experimentally. (b) The frequency of limit cycle oscillations (upper branch) is shown as a function of the reduced flow velocity.

tubes became unstable through a sub-critical Hopf bifurcation. To obtain the amplitude of the upper and lower branch oscillations, we sample the displacements of the central cylinder in the in-line and transverse directions after the cylinder motions settle into a steady state. To obtain the amplitude of the unstable limit cycle, the central cylinder was perturbed from the small-amplitude buffeting oscillations (lower branch) by giving it a measured displacement in the in-line direction. The smallest such perturbation (within $\pm$ 1.6 mm) that resulted

in a jump to a stable, large-amplitude limit cycle (upper branch) was recorded as the amplitude of the unstable limit cycle. Figure 2(b) shows that the frequency of oscillations in the upper branch does not vary significantly.

The method used to estimate the amplitude of the unstable limit cycle is appropriate if the phase space has two dimensions. For the system studied here, however, the phase space has 28 dimensions (four from each of the seven cylinders). Nevertheless, the existence of an invariant, two-dimensional subspace of the 28-dimensional phase space, that attracts all the trajectories near the equilibrium point asymptotically (i.e., a two-dimensional *center manifold*) roughly justifies the use of this method†. The center manifold theory [see e.g., Wiggins (1990)] is applicable to systems§ which, when linearized about an equilibrium point, have some eigenvalues which have zero real part and others which have negative real part. In the analysis of the model below, this is shown to be true, at the critical value of the flow velocity.

3.2. Critical Flow Velocity versus Number of Cylinders

The motion of each cylinder can be suppressed to study the effect of the number of oscillating cylinders on the critical flow velocity. Figure 3 shows the critical reduced flow velocity as a function of the number of oscillating cylinders. As the number of oscillating cylinders increases, the critical flow velocity decreases. The value of the critical reduced gap flow velocity for a single oscillating cylinder is greater than 230 (8.5 m/s upstream). Southworth & Zdravkovich (1975) briefly mention observing similar behavior in their experimental studies. The analytical model developed in this study (see Section 6) predicts the trend observed in the experiments. Blevins (1977) also shows this behavior through an analytical model.

The decrease in the critical reduced gap flow velocity with the increase in the number of oscillating cylinders suggests the role played by the coupling between the cylinders. This coupling between the cylinders is not very significant at low flow velocities as no obvious modal patterns were observed in the cylinder row in this turbulent buffeting regime. Modal structure in the turbulent buffeting emerges gradually, however, as the flow velocity is steadily increased close to the critical value. The emergence of structure indicates the presence of coupling between the cylinders.

3.3. Modal Behavior

For $U_r \geq 92$, perturbations to the buffeting oscillations result in stable large-amplitude modal oscillations of the cylinder row. The upper branch of Figure 2(a) shows the amplitude of *one* such modal oscillation. Figure 4 is a schematic illustration of all the modes observed through a video camera. We obtain the modes in Figure 4 by perturbing the turbulent buffeting of the cylinders. The modes are stable for a long period of time. For a range of reduced flow velocities, more than one stable limit cycle co-exist. We find these co-existing limit cycles by perturbing different cylinders (i.e., different initial conditions). Below, we classify the different modes of the cylinder row.

†However, it is most likely that the amplitude is underestimated by this method as only one cylinder can practically be perturbed.

§The systems are written as a set of first-order differential equations (see also footnote in Section 5.2.2).

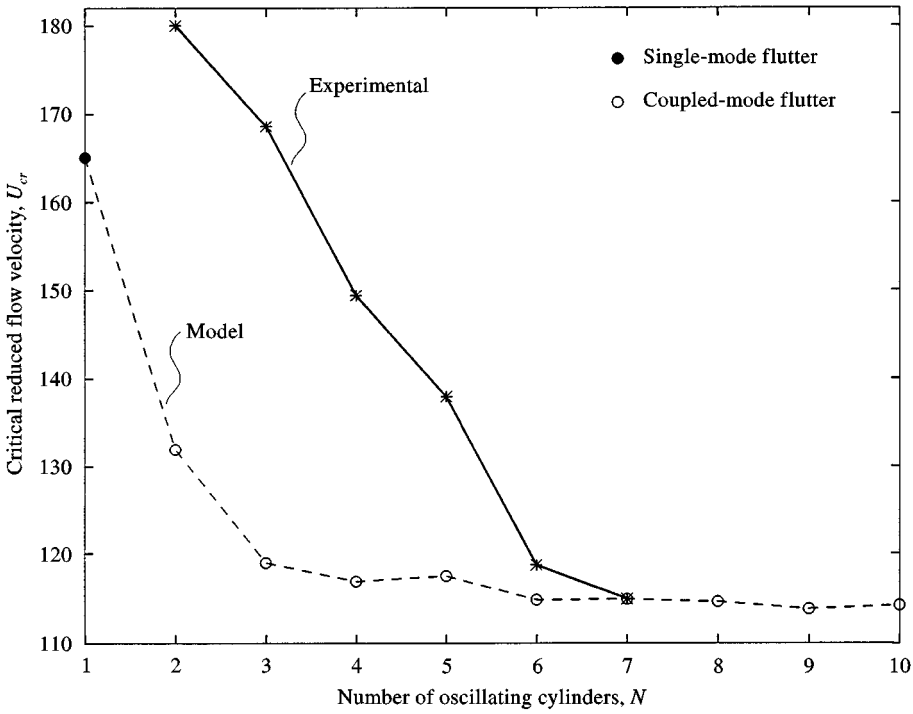

Figure 3. The variation of the critical reduced flow velocity U_{cr}, with the number of oscillating cylinders (N). For the experimental curve, the value of U_{cr} for a single oscillating cylinder could not be obtained, as it is beyond the maximum flow velocity of the experimental setup (8.5 m/s upstream corresponding to a reduced flow velocity of 230). The difference in the U_{cr} between the experiments and the model is large for all except $N = 7$. This is because the cross-coupling fluid forces which were not determined experimentally, were fitted for the U_{cr} observed in the $N = 7$ case (see Section 5).

(a) *Mode A*. This mode exists for $U_r \leq 104$. The central cylinder oscillates only in the transverse direction and the rest of the cylinders are in *anti-symmetric* motion about the central cylinder, i.e., the cylinders to the right of the central cylinder whirl in the clockwise direction, while those to the left whirl in the anti-clockwise direction. Mode A is similar to the predominant mode observed by Connors (1970) and is similar to the least stable mode of the linear model developed in this study (Figure 10).

(b) *Mode B*. This mode exists for $U_r \geq 96$ and is the only mode present at $U_r \approx 115$, the critical reduced flow velocity. The absence of symmetry in this mode implies that at high flow velocities, the coupled cylinder behavior loses symmetry. Mode B is close to a linear combination of the modes of the analytical model of this study.

(c) *Mode C*. This mode exists for low reduced flow velocities, $U_r \leq 96$. This is a nonsymmetric, *localized* mode in which the cylinders to the left of the central cylinder perform large amplitude whirling motions in the anti-clockwise direction while the cylinders to the right perform relatively smaller amplitude oscillations. Mode C is not close to any of the modes obtained by the analytical model.

(d) *Mode D*. This mode exists for low reduced flow velocities, $U_r \leq 96$. This mode seemed very close to a reflection of mode C about the y–z plane of the central cylinder, i.e., the

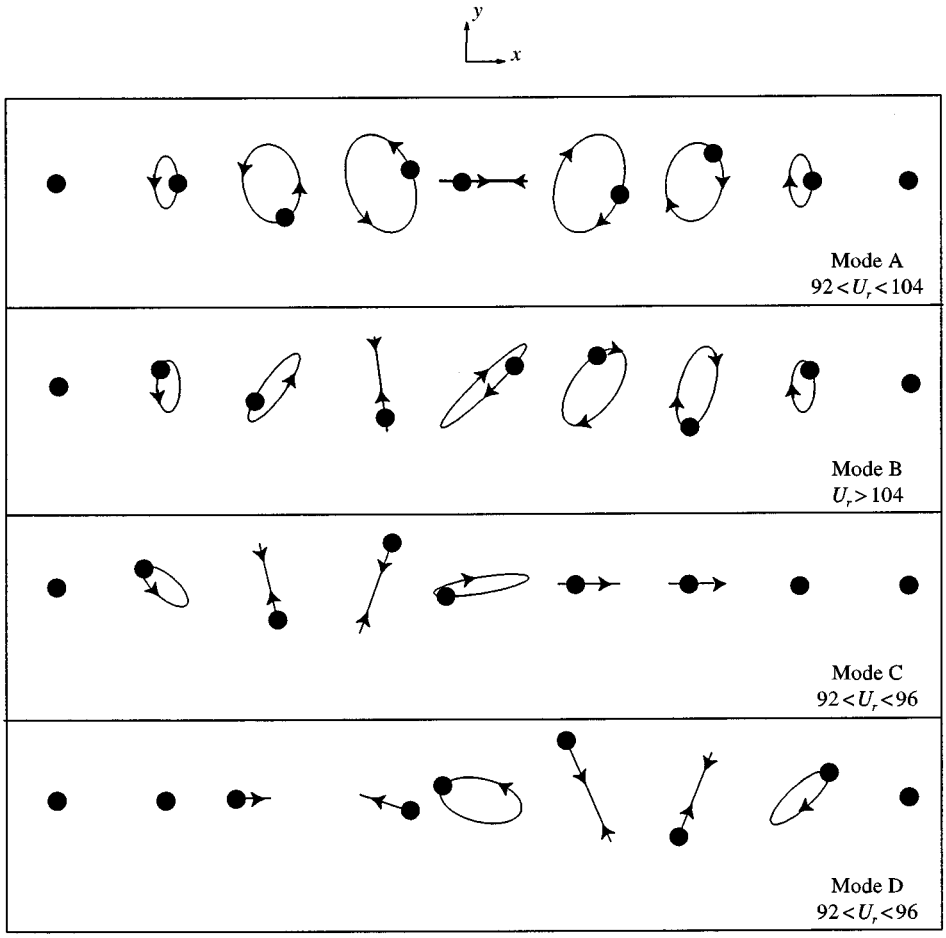

Figure 4. Schematic illustration of the stable modes of limit cycle oscillations. For some range of the flow velocity, more than one of these stable modes co-exist. These modes were observed through a video camera.

cylinders to the right of the central cylinder perform large amplitude whirling motions in the clockwise direction. Mode D is not close to any of the modes obtained by the analytical model.

Modes C and D were difficult to excite, as the set of initial conditions that excited these modes were much smaller than those for modes A and B. In all four modes, a phase difference in the positions of adjacent cylinders was observed. Although this phase difference could not be experimentally quantified (as only the central cylinder was instrumented), it was clearly observed through the video camera; [Thothadri (1996) shows the sequential frames from the motion recorded by the video camera]. In Section 5, a different representation of the modes shows them to be similar to helical waves on a string. In the ranges of the flow velocity where several modes co-exist, the modes are very sensitive to the perturbations. Moreover, on dismantling and re-assembling the

setup, mode A could not be reproduced, and slight changes were observed in the rest of the modes.

3.4. Remarks on the Experimental Results

The mode of oscillation of the cylinders in the upper branch of Figure 2(a) was similar to mode B† of Figure 4. The presence of several co-existing modes suggests that a complete bifurcation diagram would be more complicated than that shown in Figure 2(a). One very likely scenario is the presence of *secondary bifurcations* in the system. Another, is the presence of more Hopf bifurcations (sub-critical or super-critical) beyond the critical value of $U_{cr} \approx 115$, each with its own bifurcation curves. A combination of the above scenarios is also possible.

A better understanding of the co-existing limit cycles and the size of their basins of attraction could prove useful in limiting the oscillation amplitude of the cylinder row and in implementing a control algorithm for the cylinder row. For instance, the amplitudes of cylinder oscillations in localized modes C and D are much smaller than those of modes A and B; with appropriate nonlinear control we might be able to prevent the more dangerous modes (A and B) from occurring. A good understanding of the fluid forces might prove useful in designing a nonlinear model with which we could attempt at changing the sub-critical nature of the bifurcation to the more robust super-critical one.

Muntean (1995) studied the effects of the cylinder wake oscillations of the jets of fluid flowing between the cylinders with a single oscillating cylinder and reported that different patterns of coalescing jets affect the fluid damping forces on the cylinders. In this study, we have not considered the effects of jet switching as the fluid elastic instability of a row of cylinders in air is known to be due to fluid stiffness forces and not fluid damping forces (Connors 1970; Chen 1983).

4. DESCRIPTION OF THE MODEL

The goal of this part of the study was to develop a linear model to understand the modal patterns observed in the experiments and to predict the variation in the critical flow velocity with the number of oscillating cylinders. We first list the various assumptions used to obtain the model and briefly explain and justify the important ones. More details on these assumptions can be found in Thothadri (1996). Then, we present and describe the equations of motion.

4.1. Model Assumptions

In the model, the following assumptions are made.

(i) The stiffness and damping characteristics of all the cylinders are identical. (The relative errors in the stiffness constant and damping ratios were found experimentally to be less than 3% and 7·5%, respectively.)

† Figures 2 and 4 were obtained on different runs of the setup. Although the modes changed slightly in these two runs, the co-existence of limit cycles for a range of flow velocities, did not change.

(ii) *Structural* coupling of the in-line and transverse motions of any cylinder, and between adjacent cylinders are negligible.

(iii) Rocking modes are negligible. The frequency of the rocking modes are around 15 Hz in still air. The rocking modes were not observed in the experiments.

(iv) The fluid coupling is short-ranged, i.e., we assume nearest-neighbor coupling. Through a set of simple experiments, we observed that the propagation of perturbations is negligibly small beyond the nearest cylinders.

(v) The velocity profile across the cylinder row is uniform (Thothadri 1996).

(vi) The effect of vortex shedding is negligible. Vortex-induced vibrations are resonant phenomena characterized by large amplitude response over a narrow velocity range. Hence, it seems that vortex shedding cannot explain the sub-critical nature of the bifurcation. However, the effect of vortex shedding is still a debated issue. Chen *et al.* (1995) report that the modal damping of a *single* oscillating cylinder can be affected by vortex shedding.

(vii) Motion-independent fluid forces have little effect on the instability. Turbulent excitation, constant drag forces and other flow field noises constitute the motion-independent fluid forces. Although turbulent excitation can trigger fluid-elastic instability depending on its intensity, it does not explain the instability by itself. Constant drag forces are compensated in the experimental setup by re-adjusting the equilibrium position of the cylinders.

(viii) Fluid inertial forces (mostly due to added mass effect) are negligible for air, see for example Muntean (1995) and Blevins (1977).

All of these assumptions are very general and typical in most studies of such systems.

4.2. Governing Equations

With the above assumptions, the equations of motion of the nth cylinder, with respect to a frame fixed at its equilibrium position are,

$$M\begin{Bmatrix}\ddot{x}_n\\ \ddot{y}_n\end{Bmatrix}+\begin{bmatrix}C_x & 0\\ 0 & C_y\end{bmatrix}\begin{Bmatrix}\dot{x}_n\\ \dot{y}_n\end{Bmatrix}+\begin{bmatrix}K_x & 0\\ 0 & K_y\end{bmatrix}\begin{Bmatrix}x_n\\ y_n\end{Bmatrix}=\mathbf{f}_n, \tag{1}$$

where the terms on the left-hand side are the structural inertia, damping and stiffness terms per unit length of the cylinder, and $\mathbf{f}_n$ on the right-hand side is a vector containing the fluid forces per unit length on the nth cylinder in the x and y directions. The displacements of the nth cylinder are denoted by x_n and y_n.

As the motion-independent fluid forces are ignored, $\mathbf{f}_n = \mathbf{f}_n(\mathbf{x}, \dot{\mathbf{x}}, \ddot{\mathbf{x}}, U)$, where $\mathbf{x}$ is the displacement vector whose components represent the x and y displacement of all the cylinders, the overdot represents a derivative with respect to time, t, and U is the gap flow velocity. The dependence on $\ddot{\mathbf{x}}$ drops out of the equations since we assume that the fluid inertial terms are negligible. The nearest-neighbor assumption reduces the dependence of $\mathbf{f}_n$ to the motions of only the adjacent cylinders, the $(n-1)$th and $(n+1)$th cylinders.

As a result of the uniformity of the flow across the cylinder row and the periodicity of the cylinders, any set of three cylinders has a symmetry along the flow direction about the middle cylinder. The fluid force on the nth cylinder due to the relative motions of the $(n-1)$th cylinder and the $(n+1)$th cylinder (denoted by $\mathbf{f}_n^{n-1}$ and $\mathbf{f}_n^{n+1}$, respectively) are related by $\mathbf{f}_n^{n-1} = \mathbf{f}_n^{n+1}$ for the direct coupling of the x and y directions and by $\mathbf{f}_n^{n-1} = -\mathbf{f}_n^{n+1}$ for the cross-coupling between the x and y directions; see Thothadri (1996)

for details. Using these symmetry conditions and linearizing the fluid forces about the cylinder's equilibrium position, we get

$$\mathbf{f}_n = -\frac{1}{2}\rho DU\left(\begin{bmatrix} \alpha' & -\sigma' \\ -\tau' & \beta' \end{bmatrix}\begin{Bmatrix} \dot{x}_n - \dot{x}_{n-1} \\ \dot{y}_n - \dot{y}_{n-1} \end{Bmatrix} + \begin{bmatrix} \alpha' & \sigma' \\ \tau' & \beta' \end{bmatrix}\begin{Bmatrix} \dot{x}_n - \dot{x}_{n+1} \\ \dot{y}_n - \dot{y}_{n+1} \end{Bmatrix}\right)$$

$$+ \rho U^2\left(\begin{bmatrix} \alpha'' & -\sigma'' \\ -\tau'' & \beta'' \end{bmatrix}\begin{Bmatrix} x_n - x_{n-1} \\ y_n - y_{n-1} \end{Bmatrix} + \begin{bmatrix} \alpha'' & \sigma'' \\ \tau'' & \beta'' \end{bmatrix}\begin{Bmatrix} x_n - x_{n+1} \\ y_n - y_{n+1} \end{Bmatrix}\right). \tag{2}$$

The notation used is slightly different from the one used by Chen *et al.* (1993), but they formulate the equations of motion in terms of the absolute cylinder displacements, as opposed to the relative displacements used here. The single-primed quantities (α', σ', β', τ') are the fluid-damping coefficients, and the double-primed quantities (α'', σ'', β'', τ'') are the fluid-stiffness coefficients. The coefficients α'', α' couple the x-motions of adjacent cylinders and β'', β' couple y-motions.† In the following we shall refer to these as the *direct coupling coefficients*. The coefficients τ'', σ'', τ', σ' couple the x-motions of one cylinder to the y-motions of the adjacent cylinders and shall be referred to as *cross-coupling* coefficients. The quantities $\frac{1}{2}\rho DU$ and ρU^2 have been factored out to keep the fluid force coefficients nondimensional. The fluid force coefficients are independent of cylinder positions or velocities (as we have already linearized) but are generally nonlinear functions of the gap flow velocity, U.

4.3. Remarks on the Model

As the motion-dependent fluid forces on any cylinder are dependent only on its motion relative to its adjacent cylinders, any translation of the entire row of cylinders, upstream or downstream, does not change the fluid forces. This translational invariance of the motion-dependent fluid forces is inherent in our model. Most models in previous studies do not use this invariance and hence require more unknown fluid force coefficients that must be determined experimentally.

For a single cylinder oscillating in a row of rigid cylinders, this model predicts that the equations of motion in the in-line and transverse directions are uncoupled, i.e., the cross-coupling coefficients (τ'', σ'', τ', σ') drop out. So the single cylinder instability is completely governed by the direct coupling coefficients. If the instability is due to the fluid stiffness coefficients (α'', β''), the cylinder response is characterized by *static divergence*—monotonous growth without oscillations (Païdoussis *et al.* (1985). Whereas, if the instability is due to the fluid damping coefficients (α', β'), the cylinder response is asymptotically growing oscillations—known as *single-mode flutter*. The experimental measurements of the direct coupling coefficients described below show that divergence cannot occur in a single-cylinder system and that a *single-cylinder instability is due to negative damping*. To date, we have not come across a study which has observed divergence in their experiments (in a row of cylinders).‡ This important results serves to verify the model.

† Recall that, in contrast to much of the published literature, y in this paper is the *in-flow direction* — for convenience in the analysis.

‡ For *an array* of cylinders, divergence has been observed by Païdoussis *et al.* (1989).

4.4. Fluid Force Coefficients

Several previous studies have obtained the fluid forces on a cylinder row/array (Connors 1970; Tanaka & Takahara 1980; Price & Païdoussis 1984; Chen *et al.* 1993). In this study, the direct coupling coefficients were measured by using the ARMA process and the cross-coupling coefficients were determined through heuristic fits based on instability mechanisms. The procedure used is summarized in the following.

4.4.1. *Direct coupling coefficients*

As was briefly mentioned in the previous section, we measure the direct coupling coefficients from the equations of motion for a single cylinder oscillating in a row of rigid cylinders. For this single cylinder system, τ'', σ'', τ', σ' cancel out due to the anti-symmetry of the cross-coupling fluid forces. Thus, in-line and transverse equations of motion become uncoupled. The equation of motion of the cylinder in the transverse direction (x) can be written as

$$M\ddot{x} + [C_x + C_{fx}]\dot{x} + [K_x + K_{fx}]x = 0, \tag{3}$$

Where $C_{fx} = \rho DU\alpha'$ and $K_{fx} = -2\rho U^2\alpha''$ are the fluid damping and stiffness forces in the x-direction (transverse), respectively. A similar equation with β' and β'' can be written for the y-direction.

We measure the unknown fluid coefficients in equation (3) by analysing the response of the system to turbulent excitation input. The response of the system to such an input would correspond to the small amplitude buffeting oscillations (lower branch) of Figure 2(a). The turbulent excitation is a predominantly stochastic, motion-independent forcing which is seemingly the result of turbulent pressure fluctuations in the flow field and other flow noise (Blevins 1977; Muntean 1995; Thothadri 1996). We assume that the turbulent excitation forces are normally distributed, disturbance input of stochastic nature with zero mean and some variance, i.e., white noise. Although this assumption could not be verified directly, comparisons of the white noise input response of equation (3) with the measured turbulent buffeting response of the cylinder showed this assumption to be reasonable (Thothadri 1996). Equation (3) with the white noise input, $u(t)$, is written as

$$M\ddot{x} + [C_x + \rho DU\alpha']\dot{x} + [K_x - 2\rho U^2\alpha'']x = u(t). \tag{4}$$

In equation (4), $u(t)$ is known (since it is white noise) and the displacement x can be obtained experimentally by measuring the response of turbulent buffeting. In order to calculate the unknown coefficients, α', α'', we use ARMA (auto-regressive moving average) process of system identification theory; see Ljung (1987). In order to apply the ARMA process, we discretize equation (4) and from this we obtain the discrete transfer function by taking the z-transform. The details of these calculations can be found in Thothadri (1996). The entire procedure of estimating the unknowns in the transfer function was performed using Matlab's System Identification Toolbox. The algorithm in Matlab estimates the unknowns in the systems using a prediction-error method. A similar procedure was used for the y-direction also to obtain β' and β''.

4.4.2. *Comparisons of fluid force coefficients*

Figure 5 compares the direct coupling fluid force coefficients obtained above with those from Chen & Chandra (1989). Since the model developed in their study had more

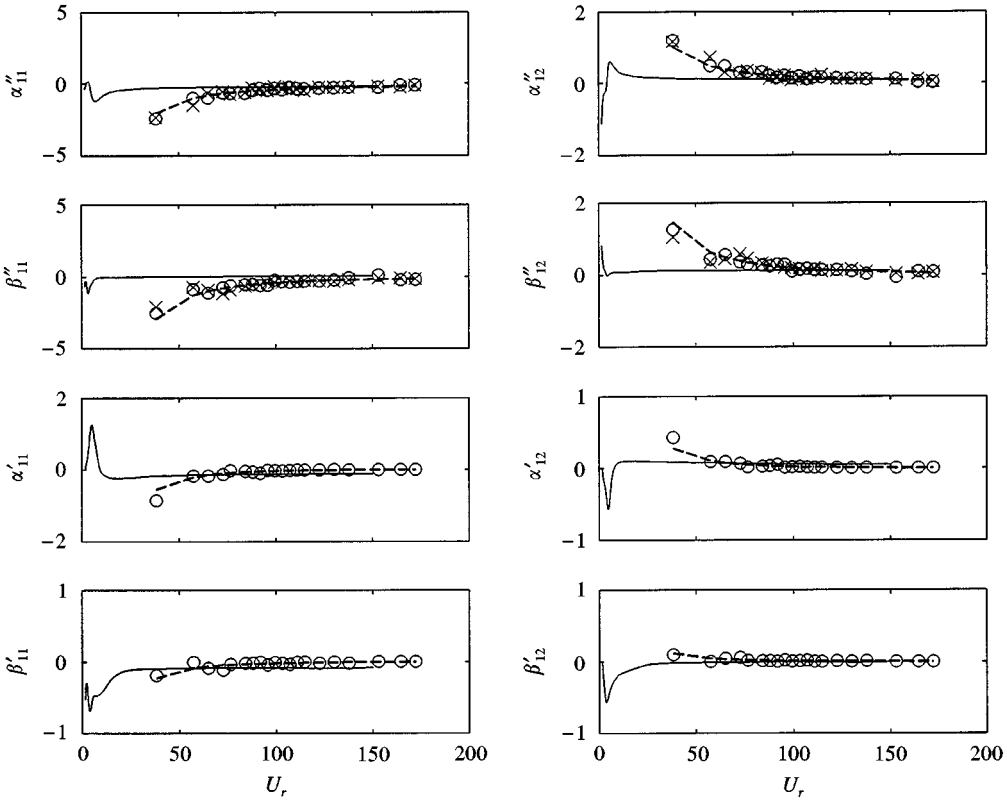

Figure 5. Comparison of the fluid force coefficients obtained in this study with those from Chen & Chandra (1989). The notation used is as in Chen & Chandra (1989). The lower indices, *ij*, imply the forces on cylinder *i* due to the motions of cylinder *j*. ○, estimated by ARMA; ×, estimated from FFT peaks (damping neglected); - - -, least-squares fit; —, Chen & Chandra (1989). The coefficients approach (nonzero) constant values for large reduced flow velocities.

independent coefficients (see Section 4.3), we could not show the comparison in the notation used in this study. Thus, we converted the above direct coupling coefficients to fit Chen & Chandra's model§. According to their notation, the lower indices *ij* imply the forces on cylinder *i* due to the motions of cylinder *j*. For instance, α'_{ij} is the fluid damping coefficient that gives the forces in the *x*-direction on the *i*th cylinder due to the *x*-directional motions of the *j*th cylinder, and similarly for β'_{ij} in the *y*-direction.

In Figure 5, the ARMA estimate and the least-squares fit closely matches that of Chen & Chandra (1989) for high flow velocities, i.e., $U_r \geq 80$. For high flow velocities, the fluid force coefficients are fairly constant, but vary significantly for small flow velocities. The fluid stiffness coefficients α'' and β'' approach constant negative values for high flow velocities and hence contribute positive stiffness force ($-2\rho U^2\alpha''$; $\alpha'' < 0$ and similarly for β''). The fluid damping coefficients, remain positive (positive damping force, $\rho DU\alpha'$) until $U_r \approx 165$ and then become slightly negative. This behavior implies that a *single cylinder* does not

§The translational invariance (see Section 4.3) gives $\alpha' = 1/2\alpha'_{11}$ and $\alpha' = -\alpha'_{12}$ and similar equations for the coefficients, α'', β'' and β'.

become unstable through divergence (since the combined stiffness of structure and fluid is always positive), but through a negative damping mechanism (single-mode flutter) with $U_{cr} \approx 165$, see Figure 3. This agrees with the results of Muntean (1995).

The fluid stiffness coefficients obtained from the peak of the power spectra of the cylinder response for various flow velocities (by neglecting damping) are also shown in Figure 5. This estimate is close to that of ARMA and the agreement improves for high flow velocities. The damping ratios of the system from equation (4) measured by ARMA are close to 10% for high flow velocities and hence do not change the frequencies much; this is not the case for smaller flow velocities (Thothadri 1996). In our study, we did not obtain the coefficients for low flow velocities ($U_r < 35$) since all of the critical flow velocities satisfy $U_{cr} \geq 115$ (see Figure 3) and the fluidelastic mechanism is dominant only for higher flow velocities.

4.4.3. *Cross-coupling coefficients*

In this study, the cross-coupling coefficients are not measured, as that would require a considerable change in the experimental setup. So we estimate them qualitatively from the instability mechanism and the critical flow velocity.

The result that the direct coupling coefficients do not lead to instability implies that the instability has to be through the cross-coupling coefficients. Previous studies (Connors 1970; Chen 1983) report that for a row of cylinders oscillating in air flow, the fluid stiffness forces are the dominant forces that lead to instability. Using this result, we assume that the fluid stiffness forces due to τ'' and σ'' are dominant and that the fluid damping forces due to τ' and σ' are ignorable, i.e., we assume $\sigma' = \tau' = 0$. We obtain heuristic fits for the coefficients σ'' and τ'' by identifying the instability boundaries and then by making the fits match critical flow velocity for seven oscillating cylinders.

To obtain the stability boundary for coupled-mode flutter, we consider a traveling wave solution to equation (2) of the form

$$\begin{Bmatrix} x_n \\ y_n \end{Bmatrix} = \begin{Bmatrix} a_1 \\ a_2 \end{Bmatrix} e^{i(qn - \omega t)} , \tag{5}$$

where $q = 2\pi\kappa P$, κ is the wave number (i.e., $2\pi P/q$ is the wavelength), ω is the angular frequency, and P (pitch) is the periodicity associated with the structure. In the above traveling wave solution, $e^{-i\omega t}$ characterizes the temporal behavior of the solution for the initial condition e^{iqn}. The quantity q is the phase diference between adjacent cylinders and characterizes the spatial distribution of the cylinders at any instant of time. Since q is within a constant ($2\pi P$) of the wavenumber κ, we refer to q as the wavenumber. Equation (2) assigns different values of ω to each q and defines a relationship $\omega = \omega(q)$. This results in the 2×2 matrix equation

$$\left[\begin{array}{c|c} \begin{array}{c} -M\omega^2 - i\omega C_x + K_x \\ -i\omega\rho DU\alpha'(1 - \cos q) \\ -2\rho U^2\alpha''(1 - \cos q) \end{array} & \begin{array}{c} i\sin q(\rho DU\sigma'(-i\omega) \\ +2\rho U^2\sigma'') \end{array} \\ \hline \begin{array}{c} i\sin q(\rho DU\tau'(-i\omega) \\ +2\rho U^2\tau'') \end{array} & \begin{array}{c} -M\omega^2 - i\omega C_y + K_y \\ -i\omega\rho DU\beta'(1 - \cos q) \\ -2\rho U^2\beta''(1 - \cos q) \end{array} \end{array}\right] \begin{Bmatrix} a_1 \\ a_2 \end{Bmatrix} = 0. \tag{6}$$

For nontrivial solutions, the determinant of the matrix in equation (6) has to be zero and this gives the dispersion relation $\omega(q)$ (Section 5 provides more details). The dispersion relation is quartic in ω, i.e., for each value of q there are four possible values of ω that satisfy the dispersion relation. If $\omega = \omega_r + i\omega_i$ satisfies the dispersion relation for a particular q, then so does $\omega = \omega_r - i\omega_i$; ω_r governs the frequency of the oscillations in a mode while ω_i governs the temporal growth or decay of the amplitude of the oscillations. A particular mode is unstable, if ω_i is greater than zero, as it leads to exponential growth of amplitude with time. If ω lies on the positive imaginary axis ($\omega_i > 0$ and $\omega_r = 0$), static instability (divergence) results. If $\omega_r \neq 0$ and $\omega_i > 0$, dynamic instability (flutter) results. As we have assumed $\sigma' = \tau' = 0$, the flutter is a *coupled-mode* mechanism due to fluid stiffness forces.

The coefficients σ'' and τ'' were chosen as linear functions of U in the coupled-mode flutter regime of equation (6). These fits were such that the experimental critical flow velocity of $U_{cr} = 115$ was matched by the model (Thothadri 1996).

5. ANALYTICAL RESULTS

We analyze the model using the theory of wave propagation in periodic structures [e.g., Brillouin 1946]. The motivation for using a wave model was to explore the spatial relationship between cylinders, that give rise to the experimentally observed modes in Figure 4. In the following, we present the results of our analyses.

5.1. Dispersion Relations

The traveling wave solution, equation (5), written compactly as $\mathbf{x} = \mathbf{a}e^{i(qn - \omega t)}$, gives $\mathbf{x}_{n+1} = \mathbf{x}_n e^{iq}$. The frequency $\omega(q)$ has a period 2π in q, i.e. $\omega(q) = \omega(q + 2\pi)$; as $q = 2\pi\kappa P$, this periodicity leads to $q(\kappa) = q(\kappa + 1/P)$. If we restrict q between $[-\pi, \pi]$, then $-1/2P \leq \kappa \leq 1/2P$, which means the wavelength $\lambda \geq 2P$. Thus, the shortest wavelength propagated by this system is equal to twice the distance between the cylinder axes and the frequency corresponding to this shortest wavelength is called the cut-off frequency. In the dispersion relation obtained from equation (6), the reduced flow velocity U_r is used as a parameter and the dispersion curve varies as the parameter is varied. Figure 6 shows the Brillouin diagram for $U_r = 115$ and for q in $[-\pi, \pi]$. Only the curves with negative real part in ω are shown.

5.2. Helical Wave Modes

5.2.1. *Traveling helical waves: infinite cylinder row*

The Brillouin diagram of Figure 6 shows the set wavenumbers propagated by the infinite row cylinder system. The initial condition given to this system, e^{iqn}, determines a set of wavenumbers and the corresponding set of frequencies. Of this set of wavenumbers, only those that are real are propagated by the system. For any practical initial condition, the complex wavenumbers have a positive imaginary part. These wavenumbers with a positive imaginary part are *spatially* attenuated and hence are not propagated. For a particular ω, the wavenumbers $\pm q$ result in two waves, traveling in opposite directions.

Figure 7 shows a wave traveling in the $+x$-direction in an infinite cylinder row. As the periodicity of the structure is in the x-direction, it is difficult to interpret the deflection of the cylinders in that direction. They are easier to interpret, if the x-directional motion of each

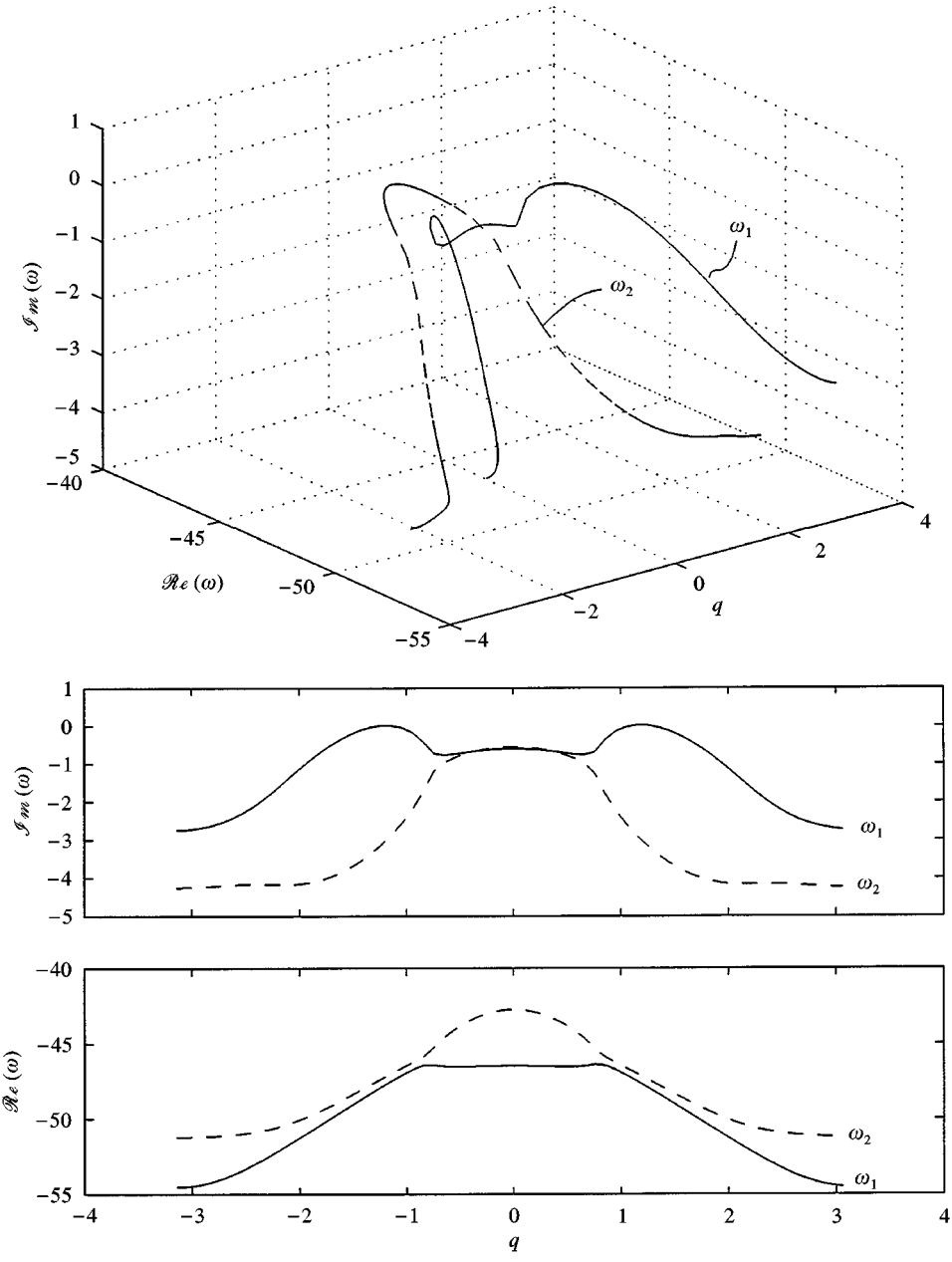

Figure 6. Brillouin diagram for $U_r \approx 115$ for q in the range $[-\pi, \pi]$. Only the curves with negative real part in ω are shown. The real part of ω corresponds to the frequency of the oscillations, while the imaginary part corresponds to the growth ($\mathcal{I}m(\omega) > 0$) or decay ($\mathcal{I}m(\omega) < 0$) of the oscillations with time. Here for some values of q, $\mathcal{I}m(\omega) > 0$ implying that the modes corresponding to these q are unstable. This diagram shows all the wave numbers propagated by the infinite cylinder row system. For the finite cylinder row system, the dispersion relation extends into imaginary q-axis.

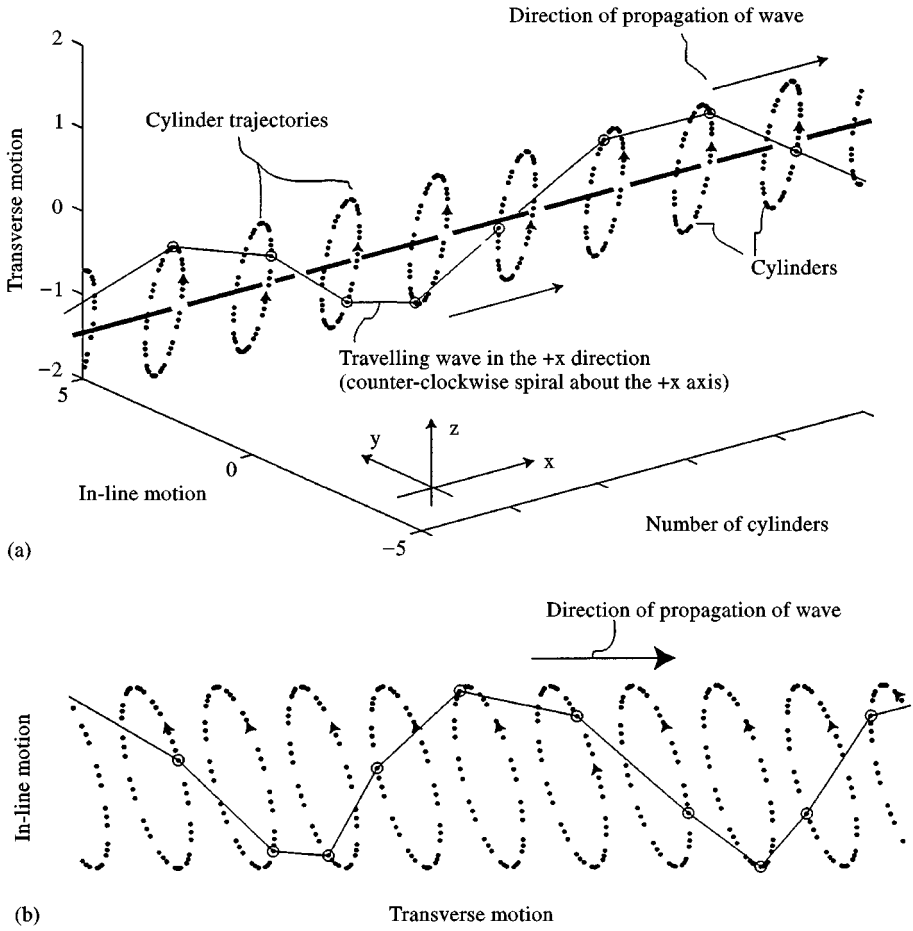

Figure 7. (a) The modal pattern of the cylinder row for the propagation of a traveling wave in the $+x$-direction at $U_r = 115$. At any time, the mode formed by the cylinder row is a helix in the counter-clockwise direction about the $+x$-axis. Each cylinder rotates about the $+x$-axis in the clockwise direction. (b) The same in the 2-D representation.

cylinder is represented along the z-axis. This representation renders the depiction of the modes to be similar to that of a string vibrating in the two transverse directions, y and z. By this representation, the wave in Figure 7 at any instant in time, is a helix that spirals around the $+x$-axis in the counter-clockwise direction. The points of constant phase advance in the $+x$-direction with velocity, ω_r/q (ω_r and $q > 0$). Moreover, each cylinder circles the $+x$-axis in the clockwise direction for this wave. The term $e^{\omega_i t}$, which controls the temporal decay or growth of the oscillations, has been omitted in Figure 7.

For the wave traveling in the $-x$-direction ($\omega_r > 0, q < 0$), the helix around the $+x$-axis is a counter-clockwise wave with the same velocity, ω_r/q. Each cylinder circles the x-axis in the counter-clockwise direction. The superposition of the two traveling waves results in a standing wave. For the standing wave, the cylinder row at any instant in time is a helix that circles around the $+x$-axis in the counter-clockwise direction. This counter-clockwise helix is to be expected as both the constituent traveling waves were so. However,

the adjacent cylinders move in the *opposite* directions about the $+x$-axis. A simple calculation shows that the helical pattern of the standing wave is due to the phase difference between the two constituent traveling waves. This phase difference depends on the coefficients τ'' and σ'' which are in turn determined by the coupled-mode flutter instability boundary described in Section 4.4.3.

The different modes of oscillations of the system become unstable at different flow velocities; the least stable mode corresponds to the mode that has the lowest critical flow velocity, i.e., the mode for which the imaginary part of ω becomes positive first, as the parameter U_r is increased.

For a cylinder row with periodic boundary condition (i.e., $\mathbf{x}_0 = \mathbf{x}_{N+1}$), the periodic boundary condition determines a discrete set of evenly spaced q's, in $[-\pi, \pi]$ and a corresponding set of ω_j's. For any initial condition, the periodic cylinder row propagates only the wavenumbers from this discrete set determined by the boundary condition. The least stable mode in this case is not necessarily the same as that for the infinite cylinder row case because not all wavelengths greater than 2P are propagated by the periodic cylinder row system.

5.2.2. *Standing helical waves: finite cylinder row*

For the fixed-ends boundary condition (i.e., $\mathbf{x}_0 = \mathbf{x}_{N+1} = \mathbf{0}$), the constraint of zero displacements for the end cylinders implies that the set of wavenumbers propagated, can no longer be purely real. The imaginary part of the wavenumbers are positive and ensures that the waves decay spatially to satisfy the boundary conditions at the ends. The dispersion relation in this case extends into the positive imaginary q-axis. The set of ω's corresponding to these q's are the eigenvalues of the system.

Figure 8 shows the locus of the eigenvalue corresponding to the least stable mode, as the parameter U_r is varied. The locus of the negative complex conjugate pair is not shown. It is seen that at the critical reduced flow velocity, one pair of eigenvalues have an exactly zero imaginary part while the others have a negative imaginary part.† Hence, the motion of the linear system at U_{cr} approaches the subspace spanned by the eigenvectors (given by $\mathbf{a}e^{iqn}$) corresponding to those eigenvalues with zero imaginary part. This subspace is invariant under a flow generated by the linearized equations. The center manifold theorem [see, e.g., Wiggins (1990)] ensures that for the full nonlinear system, there exists a subspace (center manifold) which is tangential to the subspace spanned by the eigenvectors, at the equilibrium point. The flow close to the equilibrium point approaches the center manifold asymptotically. This was used to justify the unstable limit cycle of the bifurcation diagram of Figure 2(a). The theorem also ensures that the stability of the equilibrium point in the full nonlinear equations is the same as the stability when restricted to flow on the center manifold. This fact can be used to reduce the dimensions of the system for analyzing the full nonlinear system.

Figure 9 shows a helical mode for $U_r = 90$. The central cylinder in this mode oscillates only in the in-line direction. Figure 10 shows the least stable mode for $U_r = 115$. The central cylinder in this mode oscillates only in the transverse direction and this mode is very similar to mode A of Figure 4 obtained experimentally.

† In this study, we have used $e^{-i\omega t}$ to characterize the temporal behavior of the solution instead of $e^{-\omega t}$ used in most general texts. This is responsible for the difference in reference to the real and imaginary parts.

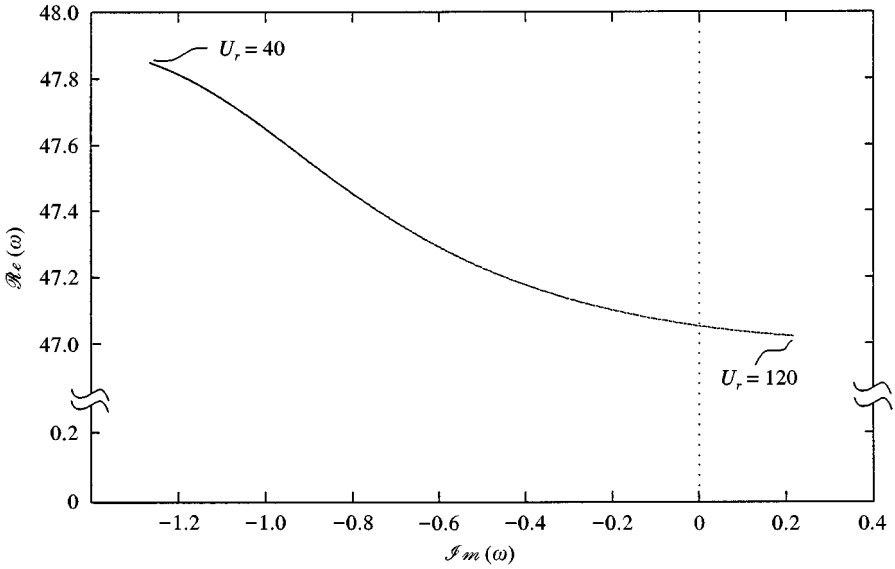

Figure 8. The locus of the least stable eigenvalue as the reduced flow velocity U_r is varied. The imaginary part of eigenvalue crosses to the positive side at $U_r = 115$. Only one of the negative complex conjugate roots is shown.

From these figures, it can be seen that all the cylinders reach the peak amplitude of their elliptical path at the same time but since the elliptical path of each of the cylinders is oriented differently, their instantaneous position acquires the shape of a helix. The cylinders on either side of the central cylinder oscillate in the opposite directions as observed experimentally (Figure 4). The motions of the cylinders on either side of the central cylinder are reflections of each other about the y–z plane of the central cylinder. All the other modes of the system are similar to modes shown in Figures 9 and 10.

6. COMPARISONS AND CONCLUDING REMARKS

The analysis of the single cylinder system shows that the motions of the cylinder in the in-line and transverse directions are uncoupled (to the linear extent) and the instability occurs through negative damping, i.e., single-mode flutter. It also verifies the widely observed fact that divergence cannot occur for the single-cylinder system in a row of cylinders.

The analysis of the multi-cylinder system provides a good understanding of the spatial modes and their relation to the instability mechanisms. The model performs quite reasonably in predicting some of the aspects of the modes. The least-stable mode shown in Figure 10, obtained by the analysis of seven-cylinder system, is similar to the experimentally observed mode A of Figure 4. Moreover, a linear combination of the modes obtained from the analysis results in a mode close to mode B. The model predicts that the cylinders on either side of the central cylinder oscillate in opposite directions, as observed experimentally. Thus, the linear modes obtained from the model are close to some of the experimentally observed spatial modes of the nonlinear system. The linear model, as expected, does not capture all the nonlinear modes observed in the experiments. The

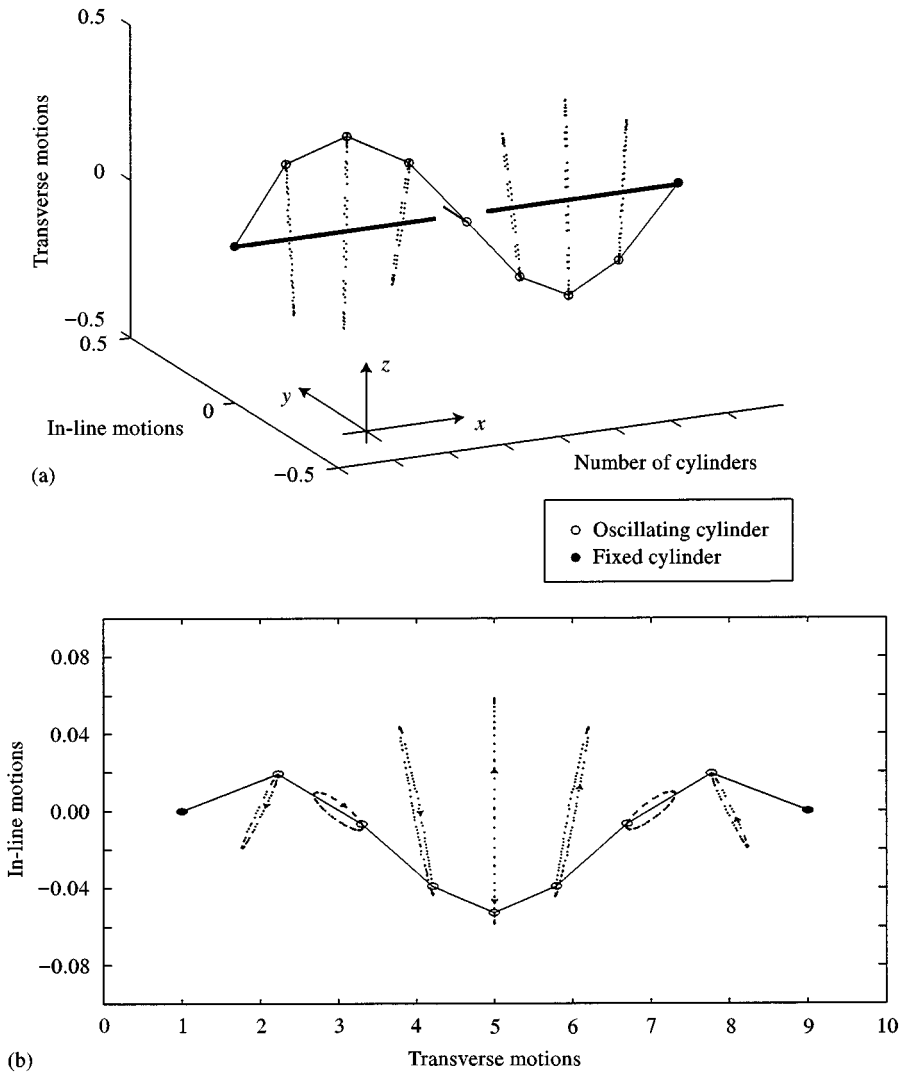

Figure 9. A modal pattern for the oscillations of the finite cylinder row (nine cylinders) at $U_r = 90$. (a) Shows that at any instant, the mode is a helix in the counter-clockwise direction. The motion of the central cylinder is only in the in-line direction. The cylinders to the left of the central cylinder rotate about the $+x$-axis in the counter-clockwise direction while those to the right rotate in the clockwise direction about the $+x$-axis. The paths of the cylinders are symmetric about the central cylinder, as can be seen from (b).

localized modes C and D of Figure 4 are not predicted by the model. As the oscillations in these localized modes have lower amplitudes, with appropriate nonlinear control, we might be able to prevent the modes with large oscillation amplitude from occurring.

Figure 3 shows the variation of the critical flow velocity with the number N, of oscillating cylinders in the tube row. A comparison of this analytical result with the experimental one indicates that the model does poorly in capturing the exact value of the critical flow velocity, except for $N = 7$. This is to be expected because the cross-coupling terms in the fluid forces were chosen to yield an accurate match for $N = 7$ only. Although the model does poorly

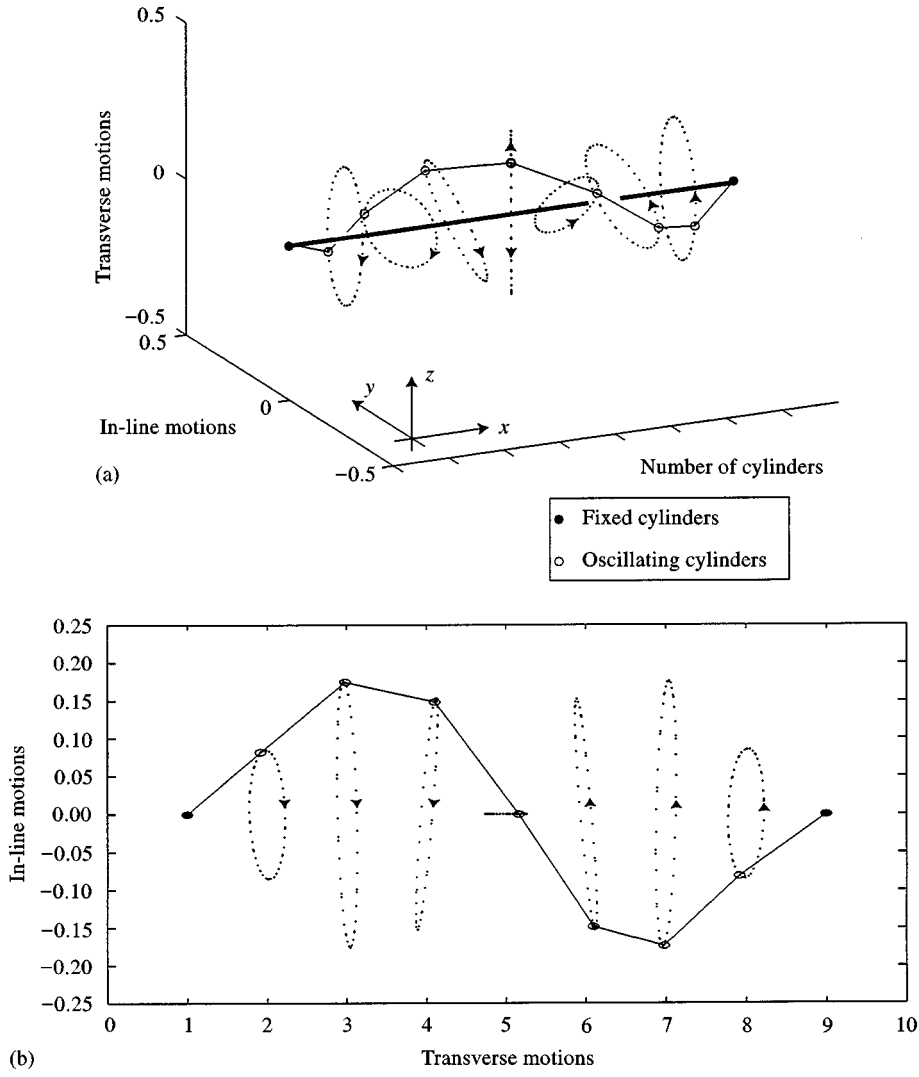

Figure 10. The *least stable* mode for $U_r = 115$. The central cylinder oscillates only in the transverse direction, and motions of the cylinders to the left and the right of the central cylinder have a reflection symmetry about the $y - z$ plane of the central cylinder. (a) Shows that the cylinders to the left rotate in the anti-clockwise direction about the $+x$-axis and those to the right rotate in the clockwise direction; the helical pattern is in the counter-clockwise direction about the $+x$-axis. (b) Shows the 2-D representation.

with the other critical velocities, it does predict the importance of coupling in reducing the critical flow velocity.

It is seen that the model performs quite well with respect to the modes but not so with respect to the critical flow velocities for various N. This suggests that a *qualitative* knowledge of the fluid forces is sufficient to obtain the modes and instability mechanisms, but a greater detail of the forces is required to be able to predict the critical flow velocities. This seems to imply that the modes and instability mechanisms are more robust to small changes in the fluid forces than the critical flow velocity.

As the linear stability analysis does not give a robust value for the critical flow velocity, a nonlinear model is necessary to develop any control scheme that aims at changing the sub-critical nature of the instability.

References

Blevins, R. D. 1977 *Flow-Induced Vibrations*. New York: Van Nostrand Reinhold Company.

Brillouin, L. 1946 *Wave Propagation in Periodic Structures*. New York: Mc Graw-Hill Book Company, Inc.

Chen, S. S. 1978 Crossflow-induced vibrations of heat exchanger tube banks. *Nuclear Engineering and Design* **47,** 67–86.

Chen, S. S. 1983 Instability mechanisms and stability criteria of a group of circular cylinders subjected to cross-flow, Part 1: Theory; Part 2: Numerical results and discussion. *ASME Journal of Vibration, Acoustics, Stress and Reliability in Design* **105,** 58,253.

Chen, S. S. 1987 A general theory for dynamic instability of tube arrays in crossflow. *Journal of Fluids and Structures*, **1,** 35–53.

Chen, S. S. 1989 Some issues concerning fluid-elastic instability of a group of circular cylinders in cross-flow. *ASME Journal of Pressure Vessel Technology* **111,** 507–518.

Chen, S. S. & Chandra, S. 1989 Fluidelastic instabilities in tube bundles exposed to nonuniform crossflow. Research Report ANL-89/13, Argonne National Laboratory.

Chen, S. S., Zhu, S. & Cai, Y. 1995 An unsteady flow theory for vortex-induced vibration. *Journal of Sound and Vibration* **184,** 73–92.

Chen, S. S., Zhu, S. & Jendrzejczyk, J. A. 1993 Motion-dependent fluid forces acting on tube arrays in crossflow. Research Report ANL-93/15, Argonne National Laboratory.

Connors, H. 1970 Fluid-elastic vibration of tube arrays excited by cross flow. In *Flow-Induced Vibration in Heat Exchangers* (ed. D. D. Reiff), pp. 42–56, New York: ASME.

Lever, J. H. & Weaver, D. S. 1982 A theoretical model for fluid-elastic instability in heat exchangers. *ASME Journal of Pressure Vessel Technology* **104,** 147–158.

Ljung, L. 1987 *System Identification: Theory for the User*. Englewood Cliffs, NJ.: Prentice-Hall.

Moon, F. C. & Holmes, P. J. 1979 A magnetoelastic strange attractor. *Journal of Sound and Vibration* **65,** 275–296.

Muntean, G. 1995 Influence of fluid wake structure on the dynamics of a flexible tube row in cross flow. Ph.D. Thesis, Cornell University.

Païdoussis, M. P. 1987 Flow-induced instabilities of cylindrical structures. *Applied Mechanics Reviews* **40,** 163–175.

Païdoussis, M. P. & Price, S. J. 1988 The mechanisms underlying flow-induced instabilities of cylinder arrays in cross flow. *Journal of Fluid Mechanics* **187,** 45–59.

Païdoussis, M. P., Price, S. J. & Mavriplis, D. 1985 A semipotential flow theory for the dynamics of cylinder arrays in cross flow. *ASME Journal of Fluids Engineering* **107,** 500–506.

Païdoussis, M. P., Price, S. J. & Mureithi, W. N. 1993 Nonlinear and chaotic dynamics of a two-degree-of-freedom analytical model for a rotated triangular aray in cross-flow. *Journal of Fluids and Structures* **7,** 497–520.

Païdoussis, M. P., Price, S. J., Nakamura, T., Mark, B. & Mureithi, W. N. 1989 Flow-induced vibrations and instabilities in a rotated-square cylinder array in cross-flow. *Journal of Fluids and Structures* **3,** 229–254.

Price, S. J. 1995 A review of theoretical models for fluid-elastic instability of cylinder arrays in cross-flow. *Journal of Fluids and Structures* **9,** 463–518.

Price, S. J. & Païdoussis, M. P. 1984 The aerodynamic forces acting on groups of two and three circular cylinders when subject to cross-flow. *Journal of Wind Engineering and Industrial Aerodynamics* **17,** 329–347.

Roberts, B. W. 1966 Low frequency, aeroelastic vibrations in a cascade of circular cylinders. Mechanical Engineering Science Monograph No. 4. London: Institution of Mechanical Engineers.

Southworth, P. J. & Zdravkovich, M. M. 1975 Cross-flow-induced vibrations of finite tube bank in in-line arrangement. *Journal of Mechanical Engineering Science* **17,** 190–198.

Tanaka, H. & Takahara, S. 1980 Unsteady fluid dynamic force on tube bundle and its dynamic effect on vibration. In *Flow-Induced Vibration of Power Plant Components* (ed. M. K. AuYang), pp. 77–92. New York: ASME.

THOTHADRI, M. 1996 Dynamics of a row of cylinders in cross flow. Master's Thesis, Cornell University.
WEAVER, D. S. & FITZPATRICK, J. A. 1987 A review of flow induced vibrations in heat exchangers. In *Proceedings of the International Conference in Flow-Induced Vibrations*, pp. 1–17. Cranfield, U.K.: BHRA.
WIGGINS, S. 1990 *Introduction to Applied Nonlinear Dynamical Systems and Chaos.* New York: Springer-Verlag.
WOODSON, H. H. & MELCHER, J. R. 1968 *Electro-mechanical Dynamics, Part* 2: *Fields, Forces, and Motion.* New York: Wiley.

APPENDIX: NOMENCLATURE

x	transverse direction
y	in-line direction
x_n, y_n	transverse and in-line displacements of the nth cylinder, respectively
P	pitch; the spacing between adjacent cylinder axes
D	diameter of the cylinders
ρ	density of air
N	number of *oscillating* cylinders in the row
M	mass per unit length of the cylinders
C_x, C_y	damping constants per unit length, in the transverse and in-line directions, respectively
K_x, K_y	stiffness constants per unit length, in the transverse and in-line directions, respectively
f_n	fluid force per unit length on the nth cylinder
f_n^i	fluid force per unit length on the nth cylinder due to the relative motions of the ith cylinder
f_x, f_y	natural frequencies of oscillation of the cylinders in the transverse and in-line directions, respectively (in Hz)
δ	damping ratio in still air for oscillations of the cylinder in both transverse and in-line directions
U_0	upstream flow velocity
U	gap flow velocity
U_r	nondimensional reduced flow velocity, U/f_yD
U_{cr}	critical reduced flow velocity
α', τ', σ', β'	fluid damping coefficients
α'', τ'', σ'', β''	fluid stiffness coefficients
α', β', α'', β''	direct coupling coefficients
τ', σ', τ'', σ''	cross-coupling coefficients
ω	angular frequency that characterizes the temporal behavior of the traveling wave solution, $\omega_r + \mathrm{i}\omega_i$
q	phase difference between adjacent cylinders, $2\pi\kappa P$
κ	wave number
t	time
$u(t)$	white noise